Toward single cell tattoos: Biotransfer printing of lithographic gold nanopatterns on live cells

Kam Sang Kwok^{1,‡}, Yi Zuo^{2,3,‡}, Soo Jin Choi^{1,‡}, Gayatri J. Pahapale¹, Luo Gu^{2,3,*}, David H. Gracias ^{1,2,4-8,*}

¹Department of Chemical and Biomolecular Engineering, Johns Hopkins University, Baltimore, Maryland 21218, United States

²Department of Materials Science and Engineering, Johns Hopkins University, Baltimore, Maryland 21218, United States

³Institute for NanoBioTechnology (INBT), Johns Hopkins University, Baltimore, Maryland 21218, United States

⁴Department of Chemistry, Johns Hopkins University, Baltimore, Maryland 21218, United States

⁵Laboratory for Computational Sensing and Robotics (LCSR), Johns Hopkins University, Baltimore, Maryland 21218, United States

⁶Sidney Kimmel Comprehensive Cancer Center (SKCCC), Johns Hopkins School of Medicine, Baltimore, Maryland 21287, United States

⁷Center for MicroPhysiological Systems (MPS), Johns Hopkins School of Medicine, Baltimore, Maryland 21287, United States

⁸Department of Oncology, Johns Hopkins School of Medicine, Baltimore, Maryland 21287, United States

* Corresponding authors: dgracias@jhu.edu, luogu@jhu.edu, <a href="mailto

Author Contributions

[‡]These authors contributed equally.

KEYWORDS: Biosensors, cell culture, hydrogels, wearables, robotics, nanoimprint

Abstract

Lithographic nanopatterning techniques like photolithography, electron-beam lithography, and nanoimprint lithography (NIL) have revolutionized modern-day electronics and optics. Yet, their application for creating nano-bio interfaces is limited by the cytotoxic and two-dimensional nature of conventional fabrication methods. Here, we present a biocompatible and cost-effective transfer process that leverages (a) NIL to define sub-300 nm gold (Au) nanopattern arrays, (b) amine functionalization of Au to transfer the NIL-arrays from a rigid substrate to a soft transfer layer, (c) alginate hydrogel as a flexible, degradable transfer layer, and (d) gelatin conjugation of the Au NIL-arrays to achieve conformal contact with live cells. We demonstrate biotransfer printing of the Au NIL-arrays on rat brains and live cells with high pattern fidelity and cell viability and observed differences in cell migration on the Au NIL-dot and NIL-wire printed hydrogels. We anticipate that this nanolithography-compatible biotransfer printing method could advance bionics, biosensing, and biohybrid tissue interfaces.

Engineers have long sought to merge nanoelectronics, nanophotonics, and stimuli-responsive materials with the human body across length scales of organs to single cells. 1.2 To create smart devices tailored to the soft, dynamic, and three-dimensional (3D) surfaces of biological systems, it is necessary to establish methods that can reliably integrate well-defined nanopatterns, such as electrode arrays, antennas, and circuits, onto living cells and tissues. In the last few decades, advances in very large-scale integration (VLSI) and micro-electromechanical systems (MEMS) have enabled the fabrication of sophisticated devices like transistors, integrated circuits, and sensors with exquisite nanoscale resolution. More recently, the assembly of materials and devices on flexible substrates that can mold to curvilinear surfaces has been achieved via laser printing, 3-5 3D printing, 6 micro pick-and-place systems, 7 and self-assembly. 8 These top-down processes, however, often utilize harsh chemicals, high temperatures, or vacuum techniques that are incompatible with living cells, tissues, and soft, aqueous materials.

To address this challenge, researchers have explored alternative approaches to creating biological interfaces, such as depositing force-mediating nanoparticles on cells or 3D bioprinting composite formulations of nanomaterials and cells.^{9–11} However, these biocompatible techniques often possess limited throughput and resolution, especially at sub-micron length scales. Yet others have shown that living cells can internalize microstructures, such as radio-frequency identification (RFID),¹² force and pressure sensors,^{13,14} barcodes,¹⁵ magnetic antennas,¹⁶ and microrobots.¹⁷ These studies demonstrate the possibility of interfacing various materials with live cells and tissues. However, a lithography-based technique for systematically integrating nanomaterials onto live cells with high spatial resolution and yield has yet to be realized.

Nanotransfer printing (nTP) offers a high throughput approach to printing large-area arrays of nanopatterns on unconventional 3D substrates, ¹⁸ such as polymers, ¹⁹ elastomers, ²⁰ and hydrogels. ²¹ For instance, Jeong *et al.* used a solvent-assisted nTP technique to print arrays of plasmonic silver nanowires on soft contact lenses for enhanced Raman signals, which enabled glucose detection at low concentrations. ²² Similarly, Ko *et al.* printed Au nanowires on hyaluronic acid film to develop smart contact lenses capable of treating Irlen syndrome. ²¹ While these nTP techniques are capable of printing large-area nanopatterns on flexible substrates in parallel, they require organic solvents (e.g. toluene, acetone), high pressure (e.g. 3 bar), or high temperatures (e.g. 45-100°C)—all of which are highly unfavorable conditions for living systems.

Here, we present a hybrid nTP process that can bond lithographically defined gold (Au) nanopatterns to live cells in physiological conditions. Our approach involves three main steps: 1) conventional thermal nanoimprint lithography (NIL) and subsequent transfer onto glass coverslips to obtain arrays of Au nanodots and nanowires, 2) amine functionalization of the Au NIL-arrays followed by alginate hydrogel casting to delaminate the Au NIL-arrays from the glass coverslip, and 3) chemical conjugation of the Au NIL-arrays with gelatin to assist transfer onto tissue or living cells followed by the dissociation of the alginate hydrogel with ethylenediaminetetraacetic acid (EDTA). In this study, we show that our approach can reliably transfer 8 by 8-mm arrays of Au nanodots (250 nm diameter) and nanowires (300 nm width) created by NIL to soft and flexible alginate hydrogels. We observed pattern-specific cell migration on the Au NIL-array printed hydrogels and optimized alginate hydrogel dissolution with EDTA to maintain high cell viability. After dissociating the alginate hydrogel transfer layer, we observed that the Au

NIL-arrays bonded to individual fibroblast cells. Overall, this approach offers a versatile strategy for seamless, tattoo-esque integration of NIL-patterns and arrays with live cells and tissues.

In the first step (Figure S1), we spin-coated a sacrificial layer of polydimethylglutarimide (PMGI, SF 6) on a silicon (Si) wafer. We created 8 by 8-mm arrays of Au nanodots and nanowires on the wafer by thermal NIL and thermal evaporation of 5 nm of chromium (Cr) as an adhesion layer and 50 nm of Au. We then spin-coated 200 nm of polymethyl methacrylate (950 PMMA, A4) as a carrier film on the nanopatterned Si wafer. We released the Au NIL-arrays from the substrate by floating the wafer on top of a positive photoresist developer (MF-26A) to dissolve the PMGI sacrificial layer. Afterward, we displaced the photoresist developer with deionized water to rinse the film and subsequently with Cr etchant (Chromium Cermet Etchant TFE) to remove the Cr. After repeating the rinsing step with deionized water, we picked up the film carefully with a glass coverslip. The choice of glass coverslips as the substrate enables efficient transfer of the Au NIL-arrays to the alginate hydrogel in the second step since Au has relatively poor adhesion to SiO₂.²³ Finally, we etched the PMMA film in oxygen plasma to obtain Au NIL-arrays on the glass coverslip. The NIL-arrays can be transferred onto glass coverslips with high fidelity, and it is noteworthy that such patterns can also be transferred onto rigid 3D shapes, such as the microparticle shown in Figure S2.

The transfer of the Au NIL-arrays to live cells and tissues requires additional criteria to be met, including flexibility, physical integrity, compatibility with cell culture media, and appropriately designed relative adhesion. Specially designed hydrogels are an alternative to rigid substrates and can also act as a sacrificial layer by reverse gelation. Alginate is

widely used for cell culture and tissue engineering due to its biocompatibility and tunable, tissue-mimetic mechanical properties. ^{24,25} Therefore, we selected alginate hydrogel as an intermediary substrate to delaminate the Au NIL-arrays from the rigid glass coverslip and affix them to cell sheets and brain tissues. A key requirement for the hydrogel assisted transfer of the Au NIL-arrays in the second step is that the adhesion between the Au NIL-array and the alginate hydrogel is significantly greater than the adhesion between the Au NIL-array and the underlying glass substrate.

We investigated the effect of surface functionalization of Au on the adhesion of the Au NIL-array to the alginate hydrogel using self-assembled monolayers of either 3mercaptopropionic acid (3-MPA) or cysteamine. Both molecules have a thiol group that can covalently bind to Au, but 3-MPA contains a negatively charged carboxylic acid end group in its deprotonated form,²⁶ while cysteamine contains a positively charged amine end group in its protonated form.^{27,28} We immersed the Au NIL-arrays in ethanol solutions containing 0.26 mM of either 3-MPA or cysteamine for an hour. We then intermixed 0.5 ml of 2.5 wt% alginate solution with 125 µl of calcium sulfate to make the alginate hydrogel with a final calcium concentration of 25 mM and cast the resulting alginate hydrogel on the Au NIL-arrays. After allowing the solution to gel for 45 minutes under a glass slide, we gently peeled off the alginate hydrogel containing the Au NIL-array from the glass coverslip and placed it pattern-side up for further characterization (Figure 1). We observed that the transfer yield of the cysteamine-functionalized Au NIL-array was approximately twice that of the 3-MPA-functionalized Au NIL-array (Figure S3). We attribute this difference to favorable electrostatic forces between the positively charged end groups of the cysteamine molecules and the negatively charged carboxyl groups of alginate.²⁹ Additionally, the SEM images (Figure 1c-d) show that this transfer process can print both NIL-dots and NIL-wires with high fidelity.

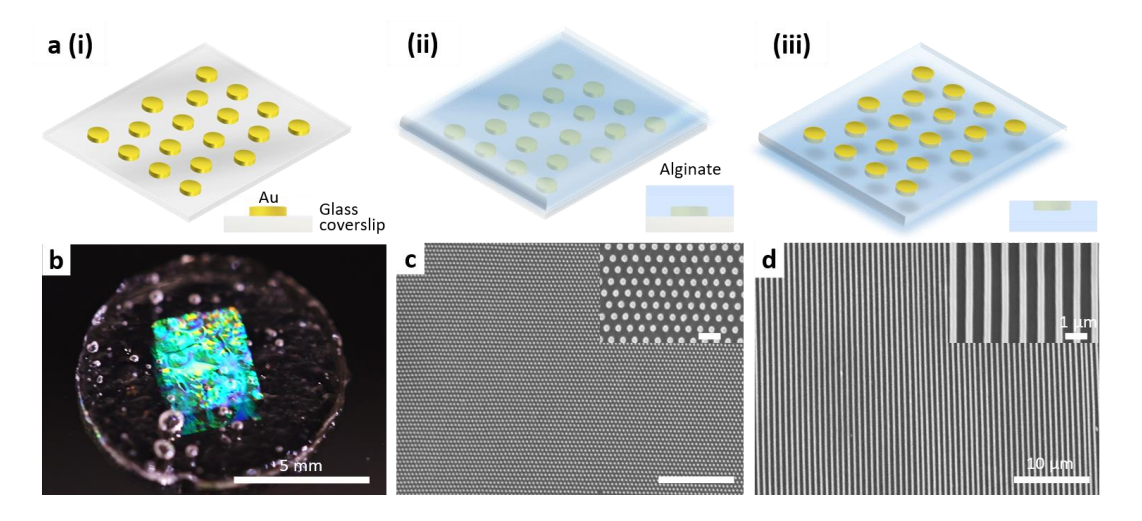


Figure 1. Schematic illustration and microscopy images showing the Au NIL-array's transfer process to the alginate hydrogel. (a) Steps for the Au NIL-array transfer to alginate hydrogel. (i) First, we transferred the Au NIL-array to a glass coverslip and then functionalized the Au with cysteamine. (ii) Next, we cast the alginate hydrogel transfer layer on top of the Au NIL-array. (iii) Then, we peeled off the alginate hydrogel containing the Au NIL-array and placed it pattern-side up. (b) Optical image of the Au NIL-array printed alginate hydrogel. (c-d) Top view SEM images of the Au (c) NIL-dot and (d) NIL-wire printed alginate hydrogel transfer layers.

Cell culture on Au NIL-array printed alginate hydrogels

We investigated the viability, migration, and morphology of embryonic mouse fibroblast cells (NIH/3T3-GFP) on two different Au nanopatterns: dots (approximately 250 nm diameter, 550 nm center-to-center spacing, 300 nm rim-to-rim spacing) and wires (approximately 300 nm wide, 450 nm spacing). As mammalian cells are known to have poor adhesion to alginate hydrogels, ³⁰ we bioconjugated gelatin to the Au NIL-array printed hydrogels prior to seeding NIH/3T3-GFP cells. The bioconjugation process (Figure S4) involves sequential functionalization of the Au surface with cysteamine and glutaraldehyde and subsequent coating with 0.1% gelatin (Bloom 300, Type A).

Glutaraldehyde contains aldehyde groups at both ends of the molecule and can bind to the amine groups in cysteamine and gelatin.³¹

Of note, certain studies have reported that glutaraldehyde can undergo acetalization with the hydroxyl groups of alginate.³² However, this crosslinking reaction occurs only under acidic conditions.³³ Conversely, glutaraldehyde exhibits rapid reactivity with amine groups and forms thermally and chemically stable crosslinks around neutral pH.34 Therefore, the reaction conditions, including pH, concentration, temperature, and reaction times, must be optimized to achieve the desired crosslinking of glutaraldehyde with cysteamine and gelatin, instead of alginate.³⁵ Approximately 24 hours after seeding the cells on the Au NIL-array printed hydrogels, we observed that the NIH/3T3-GFP cells on the NIL-wire printed hydrogel preferably migrated parallel to the nanowires, whereas those on NIL-dots exhibited random migration (Figure 2a-c). Using ImageJ, we estimated the elongation factor of the fibroblasts on the Au NIL-array printed hydrogels by measuring the long axis length over the short axis length of the cell. The elongation factor of the cells on the Au NIL-wire printed hydrogel was approximately twice that of the cells on the Au NIL-dot printed hydrogel (Figure 2d). This observation suggests that the gelatin selectively conjugated to the Au NIL-arrays, thus enhancing cell alignment and elongation on the Au NIL-wire printed alginate hydrogel compared to the Au NIL-dot printed alginate hydrogel. Also, cells on the Au NIL-dot printed hydrogel migrated about 1.4 times faster than cells on the Au NIL-wire printed hydrogel (Figure 2e). We note that the relationship between surface patterning and cell migration speed is nuanced and dependent on a variety of factors, such as relative adhesion, relative modulus, and pattern dimension and density.³⁶⁻³⁹ While many prior studies on cell migration have been carried out on stiffer substrates like glass or polydimethylsiloxane (PDMS), our method enables fabrication of soft hydrogel and physiologically relevant substrates with tunable and precisely engineered surface patterns for investigation of cell morphology and dynamics.

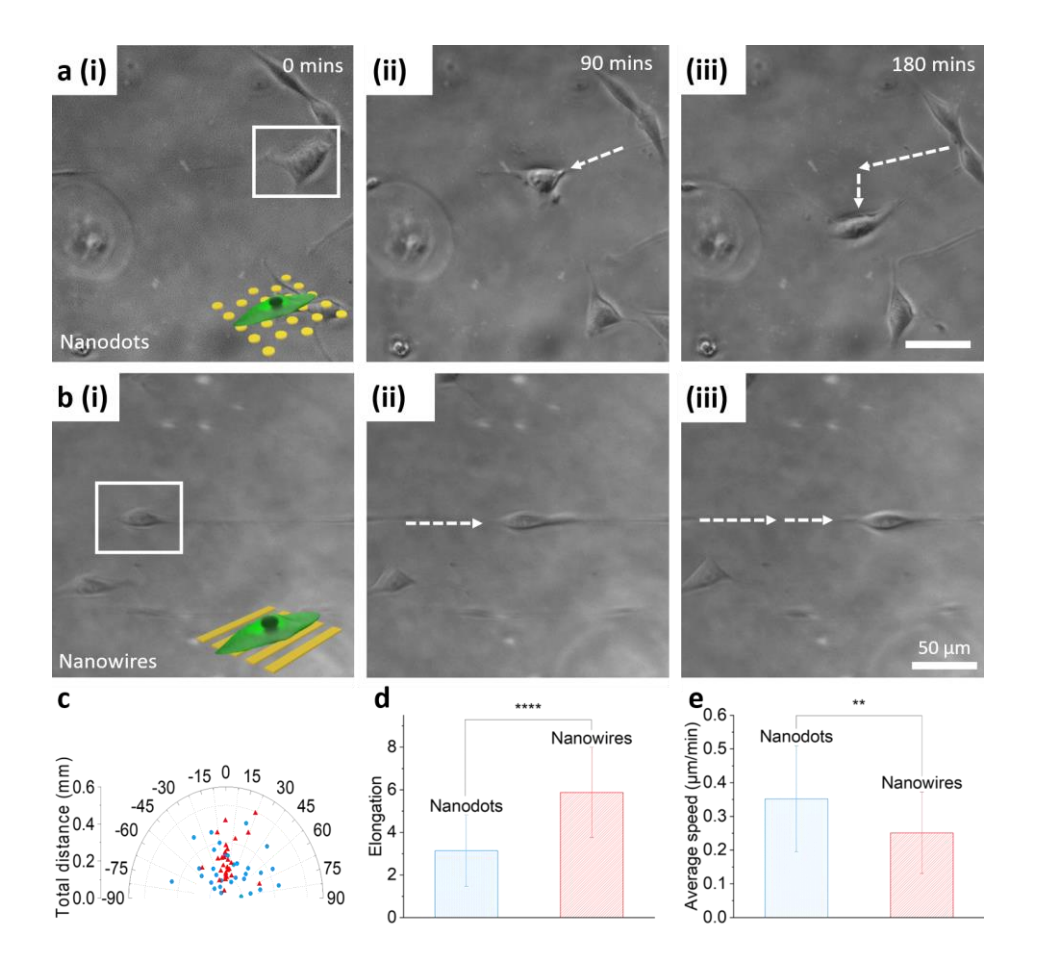


Figure 2. Characterization of NIH/3T3-GFP fibroblast migration on the Au NIL-array printed alginate hydrogels. (a) Time-lapse confocal phase images of a representative NIH/3T3-GFP cell on the Au NIL-dot printed alginate hydrogel show changing migration trajectory. (b) Time-lapse confocal phase images of a representative NIH/3T3-GFP cell on the Au NIL-wire printed alginate hydrogel show linear migration trajectory. (c) Angular distribution plot of the cell migration orientation and distance. The plot shows that cells migrated on the Au NIL-dots (blue) with no significant directional preference, whereas cells on the Au NIL-wires (red) migrated primarily along the direction of the wires. (d) Elongation factor of the cells on Au NIL-dots (blue) and Au NIL-wires (red). Cell elongation is more pronounced on Au NIL-wires. Data are presented as mean ±SD (n = 30 cells). Statistical analysis was performed using the unpaired two-sided t test. ****p<0.0001. (e) The average cell migration speed is higher on the Au NIL-dots (blue) than on the Au NIL-wires (red). Data are presented as mean ±SD (n = 30 cells). Statistical analysis was performed using the unpaired two-sided t test. **p<0.01.

Biotransfer printing Au NIL-arrays on rat brains

Alginate hydrogel is not only biocompatible with cells and tissues but can also undergo reverse gelation by metal chelates (e.g., EDTA) and specific enzymes (e.g., alginate lyases).40 Hence, it is an attractive sacrificial material for transferring the Au NILarrays onto living organs and cells. To demonstrate, we biotransfer printed Au NIL-arrays on a whole rat brain (Figure 3b-e) and on a rat brain slice (Figure S5 a). First, we dissected brains from 21-day postnatal rats and positioned the Au NIL-wire printed alginate hydrogels on the cerebral cortex of a whole brain and on a coronal brain slice. After leaving the samples in cell culture media for 2 hours (Figure 3a), we dissociated the alginate hydrogels with 20 mM EDTA. We observed that the Au NIL-wires remained bonded to the surface of the whole brain (Figure 3 d-f). In contrast, the Au NIL-wires on the coronal brain slice did not adhere and were washed away after rinsing with EDTA (Figure S5 b). Prior studies have shown that thin film patterns can conform to brain surfaces through physical adhesion forces like water capillarity or by interfacial hydrogel layers.41-44 In our experiments, the Au NIL-arrays selectively adhered to the surface of the whole rat brain, which exhibits distinct cell and matrix compositions from the coronal brain slice. This suggests that the Au NIL-array adhesion mechanism may be cell-type specific and cell adhesion-related. Further studies are needed to determine the specific adhesion factors on different cell and tissue interfaces.

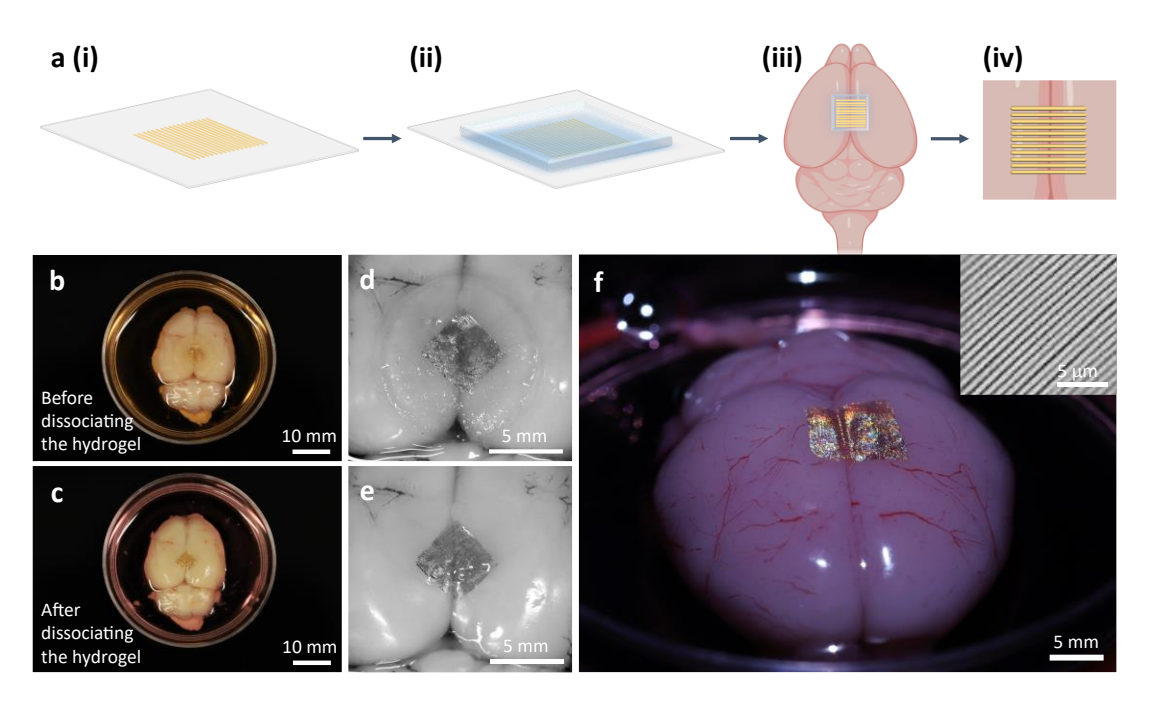


Figure 3. Schematic illustration and microscopy images showing the biotransfer printing process of Au NIL-wires on rat brains. (a) Steps for the Au NIL-array transfer to a rat brain. (i) First, we transferred the Au NIL-array to a glass coverslip and functionalized the Au surface with cysteamine. (ii) Next, we cast alginate hydrogel on top of the Au NIL-array. (iii) Then, we peeled off the alginate hydrogel containing the Au NIL-array and bioconjugated the patterned surface with gelatin before placing it on top of a rat brain. (iv) Finally, we dissociated the alginate hydrogel with 20 mM EDTA. (b-c) Optical, and (d-e) magnified images of Au NIL-wires on a rat brain (b, d) before, and (c, e) after dissociation of the alginate hydrogel with 20 mM EDTA. (f) Side view image of Au NIL-wires on a rat brain after dissociation of the alginate hydrogel transfer layer with 20 mM EDTA. The inset shows a magnified view of the Au NIL-wires on the rat brain obtained by a laser scanning microscope.

Biotransfer printing Au NIL-arrays on live NIH/3T3-GFP cell sheets

To assess the biotransfer printing capacity at the single-cell level, we transferred the Au NIL-arrays onto a monolayer of fibroblasts. The biotransfer printing process demonstrated here is inspired by cell sheet transfer with slight modifications (Figure 4a). Briefly, we cultured NIH/3T3-GFP monolayer cell sheets on Au NIL-array printed alginate hydrogels for about 24 hours. Then we flipped over the cell-seeded hydrogels onto gelatin-coated coverslips and let the cells attach to the coverslips overnight. We dissociated the alginate hydrogels by rinsing them with 20 mM EDTA for about nine

minutes. After dissociating the alginate hydrogels, we analyzed the viability of the NIH/3T3-GFP cell sheets with Au NIL-arrays using propidium iodide (PI). Using fluorescence microscopy, we qualitatively observed high cell viability with both Au NILdots and NIL-wires (Figure 4b-c). Specifically, the fibroblasts patterned with Au NIL-dots had a viability of approximately 97%, while those patterned with Au NIL-wires had a viability of approximately 98% (Figure 4d). These results indicate that this transfer printing process is biocompatible with live cells. We also observed reflective colors from the fibroblast cell sheet patterned with the Au NIL-array (Figure 4e), which suggests that the shape of the nanopattern array was retained on the cell sheet. We fixed the cell sheets patterned with Au NIL-arrays for SEM analysis and noticed that both the Au NIL-dots (Figure 4f) and NIL-wires (Figure 4g) achieved conformal contact with the cell sheets. However, when the Au NIL-arrays were biotransfer printed on cells cultured for shorter times, such as 4 hours, the patterns were either distorted or fragmented (Figure S6 b). Concurrently, we observed the presence of a thin, porous film on the cells cultured for at least 24 hours (Figure S7) but not on the cells cultured for a shorter period (Figure S6 ab). Based on these SEM images, we infer that this thin, porous film represents extracellular matrix (ECM) secreted by NIH/3T3-GFP cells and that it may be involved in facilitating adhesion between the cell sheets and the Au NIL-arrays. 45,46

Our fabrication process is not only compatible with NIL but also with microscale photolithography (Figure 4h-j). To illustrate this feature, we used photolithography and wet etching to define 200 µm-wide hexagonal patches and 200 µm-wide triangular patches of Au NIL-arrays. We then biotransfer printed the micro-patches of Au NIL-arrays onto cell sheets according to the steps shown in Figure 4a. The bioconjugation of gelatin

to the Au surface resulted in the selective growth of fibroblast cells on the micro-patches of Au NIL-arrays, as the alginate hydrogel itself does not contain any cell-adhesion ligands necessary for promoting cell attachment (Figure 4h). After dissociating the alginate hydrogel with EDTA, we observed a high yield of Au NIL-array printed micro-cell patches attached to the coverslips. The supplementary movies (Movie S1-3) show the migration of cells with patches of Au NIL-wires biotransfer printed on top of the cells. The cells with Au NIL-wires appear healthy and able to migrate indicating biocompatibility of the transfer process. Also, the movies provide evidence that the Au NIL-wires can adhere and move with cells during this 16-hour period of migration.

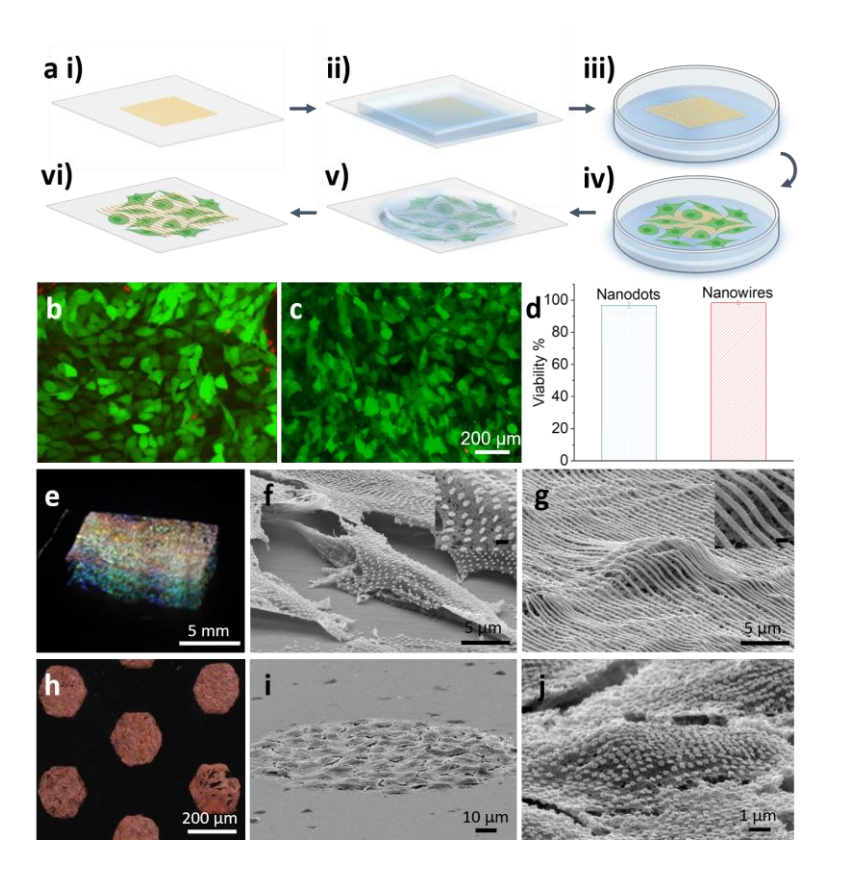


Figure 4. Characterization of the biotransfer printed Au NIL-arrays on NIH/3T3-GFP cell sheets. (a) Schematic illustration showing the steps for transferring the Au NIL-array to a cell sheet. (i) First, we transferred the Au NIL-array to a glass coverslip and functionalized the Au with cysteamine. (ii) Next, we cast alginate hydrogel on top of the Au NIL-array. (iii) Then we peeled off the alginate hydrogel containing the Au NIL-array and bioconjugated the patterned surface with gelatin. (iv) Then we seeded NIH/3T3-GFP

cells on top of the Au NIL-array printed hydrogel. (v) Next, we flipped over the cell-seeded hydrogel onto a gelatin-coated coverslip. (vi) Finally, we dissociated the alginate hydrogel with 20 mM EDTA. (b-c) Live-dead assay of NIH/3T3-GFP cells patterned with Au (b) NIL-dots or (c) NIL-wires after dissociating alginate hydrogel with 20 mM EDTA. Dead cells in red fluorescence. (d) Viability of the cells with Au NIL-dots or NIL-wires. (e) Optical image of an 8 x 8 mm array of Au NIL-arrays printed on an NIH/3T3-GFP cell sheet. (f) SEM image of Au NIL-dots on fibroblasts. (g) SEM image of Au NIL-wires on fibroblasts. (h) Optical image of the micro-cell patches with Au NIL-dots. (j) Magnified SEM image of a cell in the micro-cell patch with Au NIL-dots.

In summary, we have introduced a new approach for creating nano-bio interfaces in the form of Au NIL-arrays on live cells and tissues. Our approach utilizes molecular crosslinkers for the careful manipulation of adhesion between dissimilar materials and alginate hydrogel as both a cell culture scaffold and degradable transfer layer. We have demonstrated the ability of the Au NIL-arrays printed on physiologically relevant and ultrasoft substrates, such as hydrogels, to guide cell orientation and migration. By dissociating the alginate hydrogel with EDTA, we achieved conformal contact between the Au NIL-arrays and ex vivo rat brains as well as live cells. Noting the variation in adhesion strength among different cell types and culture methods, additional studies are needed to characterize and optimize the specific adhesion mechanisms for robust longterm bonding. Importantly, NIL patterning enables facile integration of multifunctional devices in a high throughput manner.^{47–49} Therefore, this approach could allow advanced functional optical and electronic devices, such as metamaterial arrays, plasmonic sensors, transistors, circuits, and antennas, to be imprinted on hydrogels, live cells, and tissues. 19,22,50-52 We expect this nanopatterning process, combined with various classes of materials and standard microfabrication techniques like photolithography and e-beam lithography, to open opportunities for the development of new cell culture substrates, biohybrid materials, bionic devices, and biosensors.

Supporting Information

- Experimental details including materials, methods, cell culture, cell tracking and imaging, and animal experiments; characterization of the Au NIL-arrays on alginate hydrogels and on a rat brain slice; additional SEM images of biotransfer printed Au NIL-arrays (PDF).
- Movie S1: Zoomed-in video clip of live cell imaging showing an NIH/3T3-GFP cell with Au NIL-wires biotransfer printed on top (MP4).
- Movie S2: Zoomed-in video clip of live cell imaging showing an NIH/3T3-GFP cell Au NIL-wires biotransfer printed on top (MP4).
- Movie S3: Large area video clip of live cell imaging showing NIH/3T3-GFP cells with Au NIL-wires biotransfer printed on top (MP4).

Acknowledgments

We acknowledge support from the Air Force Office of Scientific Research 21RT0264-FA9550-21-1-0284, the National Institute on Aging of the National Institutes of Health under Award Number R03AG073834, the National Science Foundation EFMA-1830893 and the Johns Hopkins University Surpass Program. The content is solely the responsibility of the authors and does not necessarily represent the official views of the funding agencies.

References

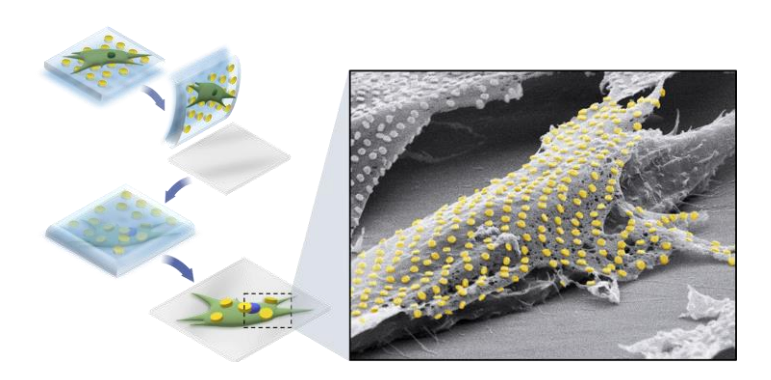
- (1) Service, R. F. The Cyborg Era Begins. *Science* **2013**, 340 (6137), 1162–1165.
- (2) Gracias, D. H. Integrated Nanotechnology 2.0: 3D, Smart, Flexible, and Dynamic [Highlights]. *IEEE Nanotechnol. Mag.* **2022**, 11–15.
- (3) Saeidpourazar, R.; Li, R.; Li, Y.; Sangid, M. D.; Lu, C.; Huang, Y.; Rogers, J. A.; Ferreira, P. M. Laser-Driven Micro Transfer Placement of Prefabricated Microstructures. *J. Microelectromech Syst.* **2012**, pp 1049–1058.
- (4) Saeidpourazar, R.; Sangid, M. D.; Rogers, J. A.; Ferreira, P. M. A Prototype Printer for Laser Driven Micro-Transfer Printing. *J. Manuf. Process.* **2012**, 14 (4), 416–424.
- (5) Li, R.; Li, Y.; Lü, C.; Song, J.; Saeidpouraza, R.; Fang, B.; Zhong, Y.; Ferreira, P. M.; Rogers, J. A.; Huang, Y. Thermo-Mechanical Modeling of Laser-Driven Non-Contact Transfer Printing: Two-Dimensional Analysis. *Soft Matter* 2012, 8 (27), 7122–7127.
- (6) Valentine, A. D.; Busbee, T. A.; Boley, J. W.; Raney, J. R.; Chortos, A.; Kotikian, A.; Berrigan, J. D.; Durstock, M. F.; Lewis, J. A. Hybrid 3D Printing of Soft Electronics. *Adv. Mater.* **2017**, 29 (40), 1703817.
- (7) Randhawa, J. S.; Leong, T. G.; Bassik, N.; Benson, B. R.; Jochmans, M. T.; Gracias, D. H. Pick-and-Place Using Chemically Actuated Microgrippers. *J. Am. Chem. Soc.* **2008**, 130 (51), 17238–17239.
- (8) Zhang, Y.; Zhang, F.; Yan, Z.; Ma, Q.; Li, X.; Huang, Y.; Rogers, J. A. Printing, Folding and Assembly Methods for Forming 3D Mesostructures in Advanced Materials. *Nat. Rev. Mater.* **2017**, 2 (4), 1–17.
- (9) Mannoor, M. S.; Jiang, Z.; James, T.; Kong, Y. L.; Malatesta, K. A.; Soboyejo, W. O.; Verma, N.; Gracias, D. H.; McAlpine, M. C. 3D Printed Bionic Ears. *Nano Lett.* **2013**, 13 (6), 2634–2639.
- (10) Di Marzio, N.; Eglin, D.; Serra, T.; Moroni, L. Bio-Fabrication: Convergence of 3D Bioprinting and Nano-Biomaterials in Tissue Engineering and Regenerative Medicine. *Front. Bioeng. Biotechnol.* **2020**, 8, 326.
- (11) Gahl, T. J.; Kunze, A. Force-Mediating Magnetic Nanoparticles to Engineer Neuronal Cell Function. *Front. Neurosci.* **2018**, 12, 299.
- (12) Yang, M. X.; Hu, X.; Akin, D.; Poon, A.; Wong, H.-S. P. Intracellular Detection and Communication of a Wireless Chip in Cell. *Sci. Rep.* **2021**, 11 (1), 1–8.
- (13) Gómez-Martínez, R.; Hernández-Pinto, A. M.; Duch, M.; Vázquez, P.; Zinoviev, K.; de la Rosa, E. J.; Esteve, J.; Suárez, T.; Plaza, J. A. Silicon Chips Detect Intracellular Pressure Changes in Living Cells. *Nat. Nanotechnol.* **2013**, 8 (7), 517–521.
- (14) Duch, M.; Torras, N.; Asami, M.; Suzuki, T.; Arjona, M. I.; Gómez-Martínez, R.; VerMilyea, M. D.; Castilla, R.; Plaza, J. A.; Perry, A. C. F. Tracking Intracellular Forces and Mechanical Property Changes in Mouse One-Cell Embryo Development. *Nat. Mater.* **2020**, 19 (10), 1114–1123.
- (15) Fernandez-Rosas, E.; Gómez, R.; Ibañez, E.; Barrios, L.; Duch, M.; Esteve, J.; Nogués, C.; Plaza, J. A. Intracellular Polysilicon Barcodes for Cell Tracking. *Small* **2009**, 5 (21), 2433–2439.
- (16) Joy, B.; Cai, Y.; Bono, D. C.; Sarkar, D. Cell Rover—a Miniaturized Magnetostrictive Antenna for Wireless Operation inside Living Cells. *Nat. Commun.*

- **2022**, 13 (1), 1–11.
- (17) Mohagheghian, E.; Luo, J.; Yavitt, F. M.; Wei, F.; Bhala, P.; Amar, K.; Rashid, F.; Wang, Y.; Liu, X.; Ji, C.; Chen, J.; Arnold, D. P.; Liu, Z.; Anseth, K. S.; Wang, N. Quantifying Stiffness and Forces of Tumor Colonies and Embryos Using a Magnetic Microrobot. *Sci. Robot.* **2023**, 8 (74), eadc9800.
- (18) Carlson, A.; Bowen, A. M.; Huang, Y.; Nuzzo, R. G.; Rogers, J. A. Transfer Printing Techniques for Materials Assembly and Micro/nanodevice Fabrication. *Adv. Mater.* **2012**, 24 (39), 5284–5318.
- (19) Jeong, J. W.; Yang, S. R.; Hur, Y. H.; Kim, S. W.; Baek, K. M.; Yim, S.; Jang, H.-I.; Park, J. H.; Lee, S. Y.; Park, C.-O.; Jung, Y. S. High-Resolution Nanotransfer Printing Applicable to Diverse Surfaces via Interface-Targeted Adhesion Switching. *Nat. Commun.* **2014**, 5 (1), 1–12.
- (20) Ahn, J.; Ha, J.-H.; Jeong, Y.; Jung, Y.; Choi, J.; Gu, J.; Hwang, S. H.; Kang, M.; Ko, J.; Cho, S.; Han, H.; Kang, K.; Park, J.; Jeon, S.; Jeong, J.-H.; Park, I. Nanoscale Three-Dimensional Fabrication Based on Mechanically Guided Assembly. *Nat. Commun.* **2023**, 14 (1), 1–10.
- (21) Ko, J.; Kang, H. J.; Ahn, J.; Zhao, Z.-J.; Jeong, Y.; Hwang, S. H.; Bok, M.; Jeon, S.; Gu, J.; Ha, J.-H.; Rho, J.; Jeong, J.-H.; Park, I. Biocompatible Nanotransfer Printing Based on Water Bridge Formation in Hyaluronic Acid and Its Application to Smart Contact Lenses. *ACS Appl. Mater. Interfaces* **2021**, 13 (29), 35069–35078.
- (22) Jeong, J. W.; Arnob, M. M. P.; Baek, K.-M.; Lee, S. Y.; Shih, W.-C.; Jung, Y. S. 3D Cross-Point Plasmonic Nanoarchitectures Containing Dense and Regular Hot Spots for Surface-Enhanced Raman Spectroscopy Analysis. *Adv. Mater.* **2016**, 28 (39), 8695–8704.
- (23) Wang, Q.; Han, W.; Wang, Y.; Lu, M.; Dong, L. Tape Nanolithography: A Rapid and Simple Method for Fabricating Flexible, Wearable Nanophotonic Devices. *Microsyst. Nanoeng.* **2018**, 4 (1), 1–12.
- (24) Chaudhuri, O.; Gu, L.; Klumpers, D.; Darnell, M.; Bencherif, S. A.; Weaver, J. C.; Huebsch, N.; Lee, H.; Lippens, E.; Duda, G. N.; Mooney, D. J. Hydrogels with tunable stress relaxation regulate stem cell fate and activity. *Nat. Mater.* **2016**, 15, 326–334.
- (25) Lee, K. Y.; Mooney, D. J. Alginate: Properties and biomedical applications. *Prog. Polym.* **2012**, 37 (1), pp 106-126.
- (26) Lesiak, A.; Banski, M.; Halicka, K.; Cabaj, J.; Zak, A.; Podhorodecki, A. pH-dependent fluorescence of thiol-coated CdSe/CdS quantum dots in an aqueous phase. *Nanotechnology* **2021**, 32 (7), 075705.
- (27) Thomas, R. C.; Houston, J. E.; Crooks, R. M.; Kim, T.; Michalske, T. A. Probing Adhesion Forces at the Molecular Scale. *J. Am. Chem. Soc.* **1995**, 117, pp 3830–3834
- (28) Atallah, C.; Charcosset, C.; Greige-Gerges, H. Challenges for cysteamine stabilization, quantification, and biological effects improvement. *J. Pharm. Anal.* **2020**, 10 (6), 499-516.
- (29) Zeeb, B.; Saberi, A. H.; Weiss, J.; McClements, D. J. Retention and Release of Oil-in-Water Emulsions from Filled Hydrogel Beads Composed of Calcium Alginate: Impact of Emulsifier Type and pH. *Soft Matter* **2015**, 11 (11), 2228–2236.
- (30) Rowley, J. A.; Madlambayan, G.; Mooney, D. J. Alginate Hydrogels as Synthetic

- Extracellular Matrix Materials. Biomaterials 1999, 20 (1), 45-53.
- (31) Ionescu R. E. Use of Cysteamine and Glutaraldehyde Chemicals for Robust Functionalization of Substrates with Protein Biomarkers-An Overview on the Construction of Biosensors with Different Transductions. *Biosensors* **2022**, 12(8), 581.
- (32) Ibrahim, N. A.; Nada, A. A.; Eid, B. M. Polysaccharide-Based Polymer Gels and Their Potential Applications. In *Polymer Gels. Gels Horizons: From Science to Smart Materials*; Thakur, V., Thakur, M. Eds.; Springer, Singapore, 2018; pp 97-126.
- (33) Pal, K. Paulson, A. T.; Rousseau, D. 14 Biopolymers in Controlled-Release Delivery Systems. In *Plastics Design Library, Handbook of Biopolymers and Biodegradable Plastics*; Ebnesajjad, S. Eds.; William Andrew Publishing, 2013; pp 329-363.
- (34) Migneault, I.; Dartiguenave, C.; Bertrand, M. J.; Waldron, K. C. Glutaraldehyde: behavior in aqueous solution, reaction with proteins, and application to enzyme crosslinking. *BioTechniques* **2004**, 37 (5), pp 790-802.
- (35) Smith, S.; Goodge, K.; Delaney, M.; Struzyk, A.; Tansey, N.; Frey, M. A Comprehensive Review of the Covalent Immobilization of Biomolecules onto Electrospun Nanofibers. *Nanomaterials* **2020**, 10 (11), 2142.
- (36) Slater, J. H.; Boyce, P. J.; Jancaitis, M. P.; Gaubert, H. E.; Chang, A. L.; Markey, M. K.; Frey W. Modulation of Endothelial Cell Migration via Manipulation of Adhesion Site Growth Using Nanopatterned Surfaces. *ACS Appl. Mater. Interfaces.* **2015**, 7 (7), 4390-4400.
- (37) Liu, Q.; Zheng, S.; Ye, K.; He, J.; Shen, Y.; Cui, S.; Huang, J.; Gu, Y.; Ding, J. Cell migration regulated by RGD nanospacing and enhanced under moderate cell adhesion on biomaterials. *Biomaterials* **2020**, 263 (2020): 120327.
- (38) Kim, J.; Bae, W. G.; Kim, Y. J.; Seonwoo, H.; Choung, H. W.; Jang K. J.; Park S.; Kim B. H.; Kim H. N.; Choi K. S.; Kim M. S.; Choung P. H.; Choung Y. H.; Chung J. H. Directional matrix nanotopography with varied sizes for engineering wound healing. *Adv. Healthc. Mater.* **2017**, 6(19): 1700297.
- (39) Kim, D.-H.; Wirtz, D. Focal Adhesion Size Uniquely Predicts Cell Migration. *FASEB J.* **2013**, 27 (4), 1351–1361.
- (40) Freedman, B. R.; Uzun, O.; Luna, N. M. M.; Rock, A.; Clifford, C.; Stoler, E.; Östlund-Sholars, G.; Johnson, C.; Mooney, D. J. Degradable and Removable Tough Adhesive Hydrogels. *Adv. Mater.* **2021**, 33 (17), e2008553.
- (41) Kim, D.-H.; Viventi, J.; Amsden, J. J.; Xiao, J.; Vigeland, L.; Kim, Y.-S.; Blanco, J. A.; Panilaitis, B.; Frechette, E. S.; Contreras, D.; Kaplan, D. L.; Omenetto, F. G.; Huang, Y.; Hwang, K.-C.; Zakin, M. R.; Litt, B.; Rogers, J. A. Dissolvable Films of Silk Fibroin for Ultrathin Conformal Bio-Integrated Electronics. *Nat. Mater.* **2010**, 9 (6), 511–517.
- (42) Viventi, J.; Kim, D.-H.; Vigeland, L.; Frechette, E. S.; Blanco, J. A.; Kim, Y.-S.; Avrin, A. E.; Tiruvadi, V. R.; Hwang, S.-W.; Vanleer, A. C.; Wulsin, D. F.; Davis, K.; Gelber, C. E.; Palmer, L.; Van der Spiegel, J.; Wu, J.; Xiao, J.; Huang, Y.; Contreras, D.; Rogers, J. A.; Litt, B. Flexible, Foldable, Actively Multiplexed, High-Density Electrode Array for Mapping Brain Activity in Vivo. *Nat. Neurosci.* 2011, 14 (12), 1599–1605.

- (43) Oribe, S.; Yoshida, S.; Kusama, S.; Osawa, S.-I.; Nakagawa, A.; Iwasaki, M.; Tominaga, T.; Nishizawa, M. Hydrogel-Based Organic Subdural Electrode with High Conformability to Brain Surface. *Sci. Rep.* **2019**, 9 (1), 13379.
- (44) Yang, Q.; Hu, Z.; Rogers, J. A. Functional Hydrogel Interface Materials for Advanced Bioelectronic Devices. *Acc. Mater. Res.* **2021**, 2 (11), 1010–1023.
- (45) Chlenski, A.; Guerrero, L. J.; Salwen, H. R.; Yang, Q.; Tian, Y.; La Madrid, A. M.; Mirzoeva, S.; Bouyer, P. G.; Xu, D.; Walker, M.; Cohn, S. L. Secreted Protein Acidic and Rich in Cysteine Is a Matrix Scavenger Chaperone. *PLoS One* **2011**, 6 (9), e23880.
- (46) Franco-Barraza, J.; Beacham, D. A.; Amatangelo, M. D.; Cukierman, E. Preparation of Extracellular Matrices Produced by Cultured and Primary Fibroblasts. *Curr. Protoc. Cell Biol.* **2016**, 71 (1), 10.9.1–10.9.34.
- (47) Zhang, M.; Pacheco-Peña, V.; Yu, Y.; Chen, W.; Greybush, N. J.; Stein, A.; Engheta, N.; Murray, C. B.; Kagan, C. R. Nanoimprinted Chiral Plasmonic Substrates with Three-Dimensional Nanostructures. *Nano Lett.* **2018**, 18 (11), 7389–7394.
- (48) Zang, F.; Su, Z.; Zhou, L.; Konduru, K.; Kaplan, G.; Chou, S. Y. Ultrasensitive Ebola Virus Antigen Sensing via 3D Nanoantenna Arrays. *Adv. Mater.* **2019**, 31 (30), e1902331.
- (49) Qi, J.; Ding, W.; Zhang, Q.; Wang, Y.; Chen, H.; Chou, S. Y. Over 100% Light Extraction Enhancement of Organic Light Emitting Diodes Using Flat Moire Micro-Lens Array Fabricated by Double Nanoimprint Lithography Over a Large Area. *arXiv* (*Physics, Optics*), January 31, 2023. http://arxiv.org/abs/2302.00066 (accessed 2023-05-25).
- (50) Rodrigo, D.; Tittl, A.; Ait-Bouziad, N.; John-Herpin, A.; Limaj, O.; Kelly, C.; Yoo, D.; Wittenberg, N. J.; Oh, S.-H.; Lashuel, H. A.; Altug, H. Resolving Molecule-Specific Information in Dynamic Lipid Membrane Processes with Multi-Resonant Infrared Metasurfaces. *Nat. Commun.* **2018**, 9 (1), 1–9.
- (51) Zhang, W.; Chou, S. Y. Fabrication of 60-Nm Transistors on 4-In. Wafer Using Nanoimprint at All Lithography Levels. *Appl. Phys. Lett.* **2003**, 83 (8), 1632–1634.
- (52) Zhang, W.; Ding, F.; Li, W.-D.; Wang, Y.; Hu, J.; Chou, S. Y. Giant and Uniform Fluorescence Enhancement over Large Areas Using Plasmonic Nanodots in 3D Resonant Cavity Nanoantenna by Nanoimprinting. *Nanotechnology* **2012**, 23 (22), 225301.

TOC Graphic



Supporting information

Toward single cell tattoos: Biotransfer printing of lithographic gold nanopatterns on live cells

Kam Sang Kwok^{1,‡}, Yi Zuo^{2,3,‡}, Soo Jin Choi^{1,‡}, Gayatri J. Pahapale¹, Luo Gu^{2,3,*}, David H. Gracias ^{1,2,4-8,*}

¹Department of Chemical and Biomolecular Engineering, Johns Hopkins University, Baltimore, Maryland 21218, United States

²Department of Materials Science and Engineering, Johns Hopkins University, Baltimore, Maryland 21218, United States

³Institute for NanoBioTechnology (INBT), Johns Hopkins University, Baltimore, Maryland 21218, United States

⁴Department of Chemistry, Johns Hopkins University, Baltimore, Maryland 21218, United States

⁵Laboratory for Computational Sensing and Robotics (LCSR), Johns Hopkins University, Baltimore, Maryland 21218, United States

⁶Sidney Kimmel Comprehensive Cancer Center (SKCCC), Johns Hopkins School of Medicine, Baltimore, Maryland 21287, United States

⁷Center for MicroPhysiological Systems (MPS), Johns Hopkins School of Medicine, Baltimore, Maryland 21287, United States

⁸Department of Oncology, Johns Hopkins School of Medicine, Baltimore, Maryland 21287, United States

* Corresponding authors: dgracias@jhu.edu, luogu@jhu.edu, <a href="mailto

Author Contributions

[‡]These authors contributed equally.

Fabrication of the Au NIL-arrays on glass coverslips

We fabricated the Au nanopattern arrays via nanoimprint lithography (NIL). Briefly, we spin-coated a layer of polymethylglutarimide (PMGI SF6, Kayaku Advanced Materials) as the sacrificial layer on a silicon (Si) wafer. Then we spin-coated a layer of NIL resist (mr-I 7030, Micro Resist Technology) with a thickness of 350 nm and thermally imprinted the nanopatterns using a Nanonex Advanced Nanoimprint Tool NX-B200 with a pressure of 350 psi at 130 °C. We used a commercial, low-cost Si master stamp (LightSmyth grating) of two kinds to create nanodots (approximately 250 nm diameter, 550 nm center-to-center spacing, 300 nm rim-to-rim spacing) and nanowires (approximately 300 nm width, 450 nm spacing). After imprinting, we etched away the residual NIL resist with oxygen plasma at 60 W for 2 minutes. We used thermal evaporation to deposit 50 nm of Au with a 5 nm-thick Cr layer underneath to improve adhesion to the nanopatterned wafer. After deposition, we sonicated the sample in acetone to completely dissolve the NIL resist and obtained a large-area array (8 by 8 mm) of Au nanopatterns on the Si wafer.

We spin-coated a layer of polymethyl methacrylate (950 PMMA A4) on top of the Au NIL-array as a carrier film. We released the Au NIL-array from the Si wafer by dissolving the PMGI sacrificial layer in a positive photoresist developer (MF-26A). To retain the shape of the nanopatterns, it is important to keep the thin film floating on the surface of the liquid for these steps. We rinsed the film with water by displacing the photoresist developer with deionized (DI) water three times. Then we etched the Cr in Cr etchant (Cr Cermet Etchant TFE, Transene) and repeated the rinsing step with water. Afterward, we picked up the film from the water-air interface using a glass coverslip. After air-drying the film, we etched the PMMA film in oxygen plasma at 60 W for 30 minutes.

Alginate hydrogel preparation

We used sodium alginate with high guluronic acid block content (average MW 177kDa, I1G, KIMICA) to fabricate the alginate hydrogel based on a published method. Briefly, we purified alginate by dialyzing it against DI water for 3 days with a 3500 MWCO membrane. Afterward, we used activated charcoal and sterile filtration to purify the alginate. We lyophilized the purified alginate for 4-5 days and stored it at -20°C until needed.

Cell culture

We cultured the NIH/3T3-GFP cells (kindly provided by Dr. Yun Chen at Johns Hopkins University) in standard DMEM (Gibco) with 10% fetal bovine serum (HyClone) and 1% penicillin/streptomycin (Gibco). The cells were cultured in a humidified incubator at 37 °C with 5% CO₂, kept at sub-confluency, and passaged every 2-3 days.

Transfer of the Au NIL-arrays to cell sheets and rat brains

We transferred the Au NIL-arrays from the glass coverslips onto cell sheets and tissues using alginate hydrogel as a biocompatible and sacrificial transfer layer. To facilitate the delamination of the Au NIL-array from the glass coverslip, we enhanced relative adhesion to the alginate hydrogel by chemically modifying the Au surface with a self-assembled monolayer of cysteamine. We immersed the Au NIL-array in a 0.26 mM cysteamine ethanol solution for an hour. Then we prepared the alginate hydrogel by mixing 0.5 ml of the 2.5 wt% alginate solution with 125 µl of calcium sulfate to make the alginate hydrogel with a final calcium concentration of 25 mM. We obtained a homogenous mixture by loading each solution in a syringe and mixing with a dual Luer-lock connector. Then we cast the alginate hydrogel on the Au NIL-array and allowed the solution to gel for 45 minutes under a glass slide with 1 mm-thick spacers. Afterward, we carefully peeled off the alginate hydrogel containing the Au NIL-array from the glass coverslip and placed it pattern-side up in a petri dish. We sterilized the hydrogel by placing it under UV light for an hour and made sure to immerse it in excess CaCl₂ solution to prevent dehydration. Then we repeated the cysteamine functionalization step and rinsed the alginate hydrogel three times with DI water. To bind the gelatin molecules, we immersed the Au NIL-array in a 17.6 mM glutaraldehyde water solution for 30 minutes and rinsed the hydrogel three times with DI water. Next, we immersed the hydrogel in a 0.1% gelatin (Bloom 300, Type A) phosphate-buffered saline solution for an hour and aspirated the excess solution. We used the same gelatin coating procedure to obtain the gelatin-coated glass coverslips. After seeding NIH/3T3-GFP cells on the Au NIL-array printed alginate hydrogel, we placed it in an incubator for 24 hours. To obtain the Au NIL-array printed cells, we picked up the cell-seeded hydrogel and flipped it over onto a gelatin-coated coverslip so that the cells were in direct contact with the gelatin-coated coverslip. We allowed the cells to attach to the gelatin-coated coverslip overnight and finally dissociated the alginate hydrogel by rinsing it with 20 mM of EDTA for about 9 minutes. For the transfer of the Au NIL-arrays to rat brains, we repeated the same alginate hydrogel casting and gelatin conjugation steps. Then we placed the Au NIL-array printed alginate hydrogel on top of the brain tissue so that the Au NIL-array was in direct contact with the tissue surface. After leaving the samples in cell culture media for about 2 hours, we dissociated the alginate hydrogel by rinsing it with 20 mM EDTA for about 9 minutes.

Cell tracking and imaging

We used a Nikon TE2000 microscope with 10X objective lens to capture cell movement over 14 hours at 5-minute intervals. During imaging, cells were maintained on a temperature and CO₂-controlled stage in an incubator at 37 °C and 5% CO₂. We used CellTracker software to record cell migration paths and calculate cell migration speed.²

The inset in Figure 3f was obtained using a Keyence laser scanning microscope VK-X100.

Animal experiments

Sprague Dawley rats were purchased from Charles River and Taconic Biosciences, and the animals were bred and housed at Johns Hopkins animal facilities. All animal procedures and experiments were performed in accordance with guidelines set by the National Institutes of Health and the Johns Hopkins University Animal Care and Use Committee (ACUC). Postnatal 21-day rats were euthanized using carbon dioxide (CO₂). Rats were further subjected to cervical dislocation following euthanasia by CO₂ inhalation. Decapitation was performed, and brains were dissected for follow-up experiments.

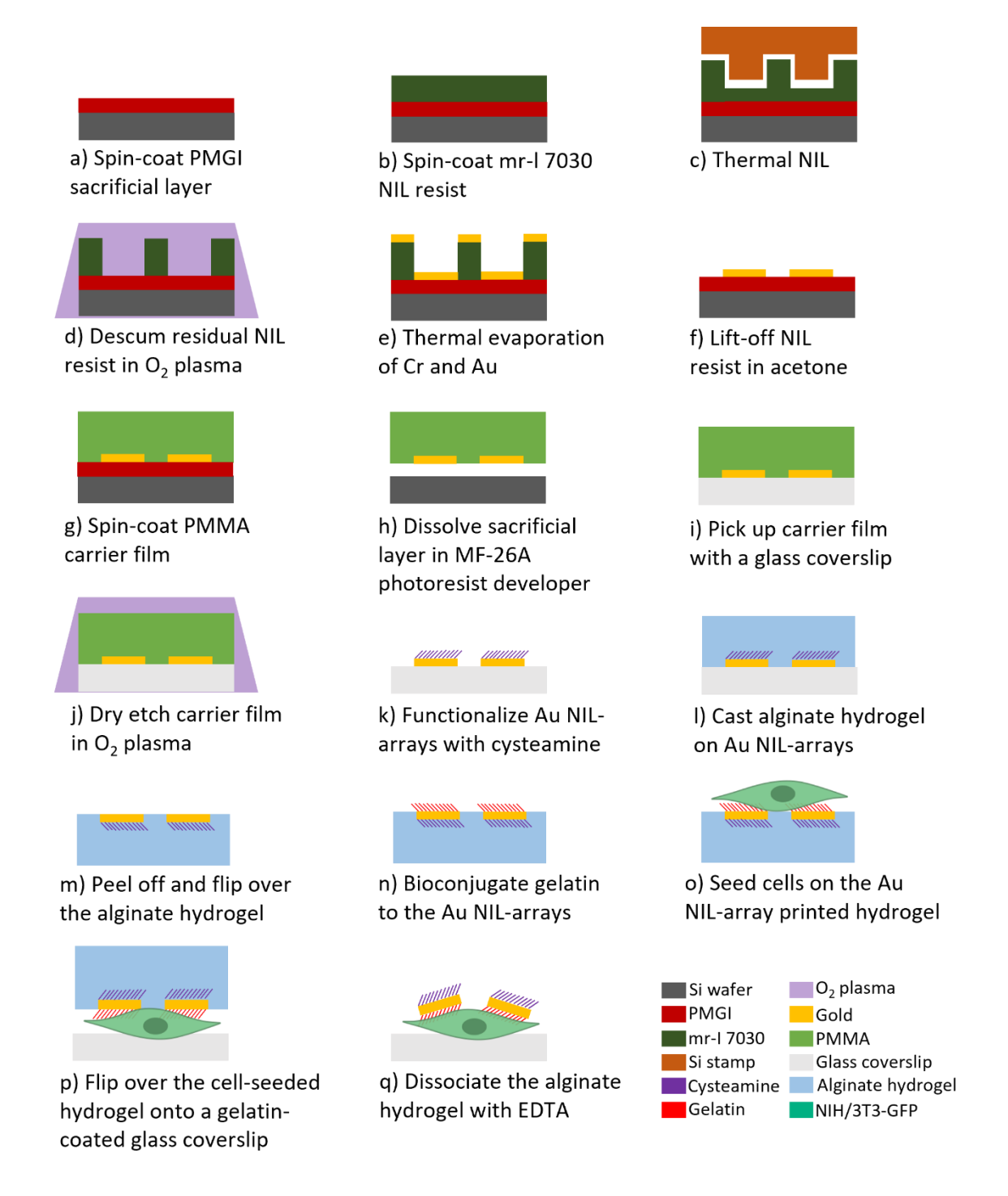


Figure S1. Schematic illustration showing the step-by-step fabrication of the Au NIL-arrays on Si wafers and subsequent transfer onto glass coverslips and cell sheets. The main steps include (a) spin-coating the sacrificial layer (PMGI) on a Si wafer, (b) spin-coating the NIL resist (mr-I 7030), (c) thermal NIL using a Si stamp, (d) descumming the residual NIL resist with oxygen plasma, (e) thermally evaporating 5 nm of Cr and 50 nm of Au, (f) lifting off the NIL resist in acetone, (g) spin-coating the carrier film (PMMA), (h) dissolving the sacrificial layer in positive photoresist developer (MF-26A) and Cr in Cr

etchant (Cr Cermet Etchant TFE) followed by rinsing with water, (i) manually picking up the Au NIL-array from the water-air interface using a glass coverslip, (j) removing the carrier film using an oxygen plasma, (k) functionalizing the Au NIL-array with cysteamine, I) casting alginate hydrogel on the Au NIL-array, m) peeling off the Au Nil-array printed alginate hydrogel from the glass coverslip and placing it pattern-side up, n) bioconjugating gelatin to the Au NIL-array according to the process detailed in Figure S4, o) seeding NIH/3T3-GFP cells on the Au NIL-array printed hydrogel and culturing for 24 hours, p) flipping over the cell-seeded hydrogel onto a gelatin-coated glass coverslip, and q) dissociating the alginate hydrogel with 20 mM EDTA to obtain the Au NIL-array printed cells.

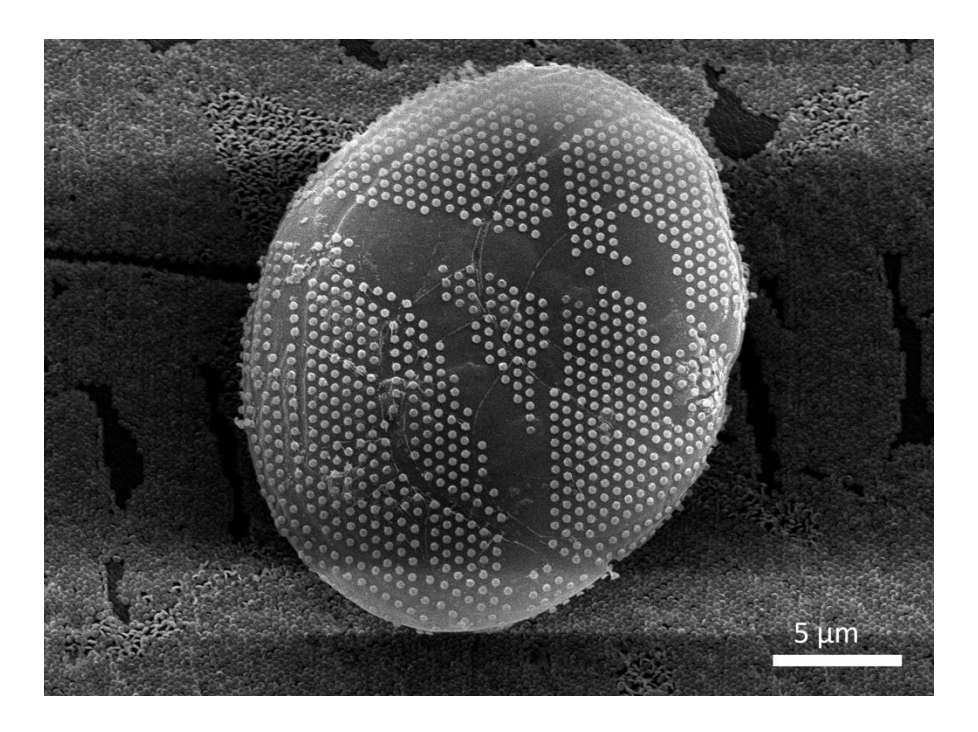


Figure S2. SEM image of Au NIL-dots biotransfer printed on the surface of a 3D microparticle.

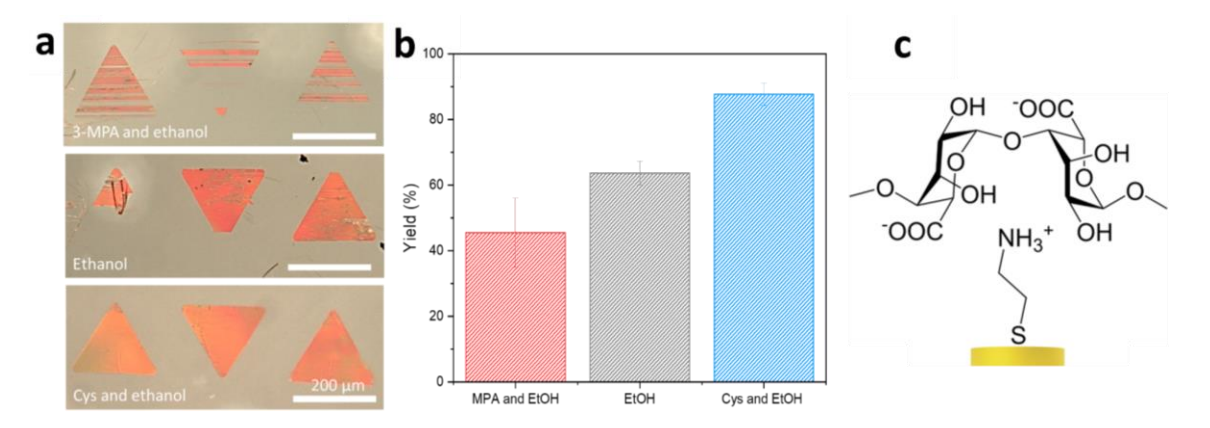


Figure S3. Characterization of the Au NIL-arrays on alginate hydrogels. a) Optical images of the Au NIL-arrays functionalized with 3-mercaptopropionic acid and ethanol (top), ethanol (middle), or cysteamine and ethanol (bottom). b) Transfer yield of the Au NIL-arrays functionalized with different molecules from the glass coverslips to the alginate hydrogels. c) Proposed mechanism for enhancing the transfer yield of the Au NIL-arrays to the alginate hydrogel with positively charged cysteamine.

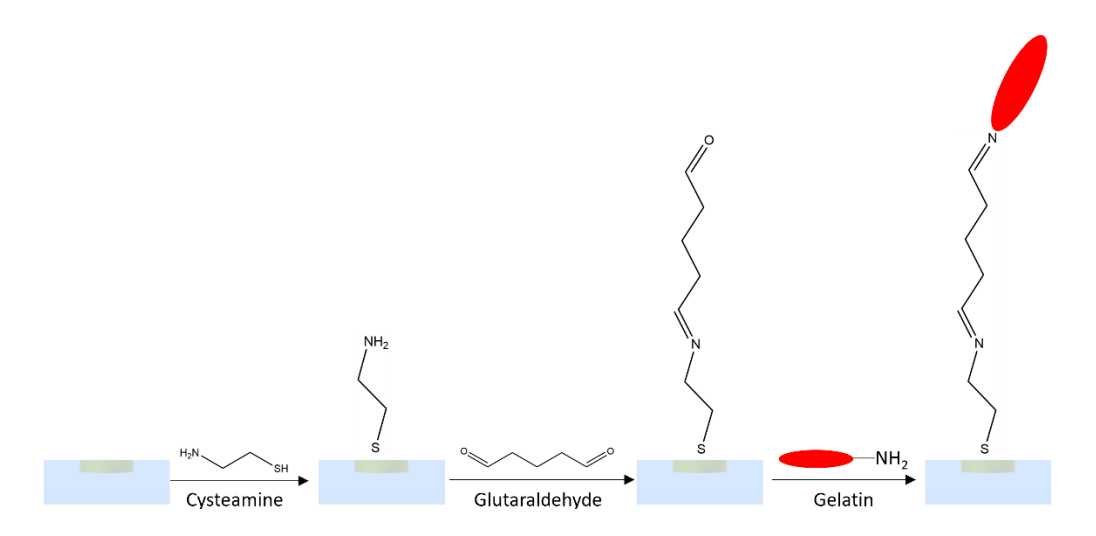


Figure S4. Schematic illustration showing the steps for the bioconjugation of gelatin to the Au NIL-arrays.

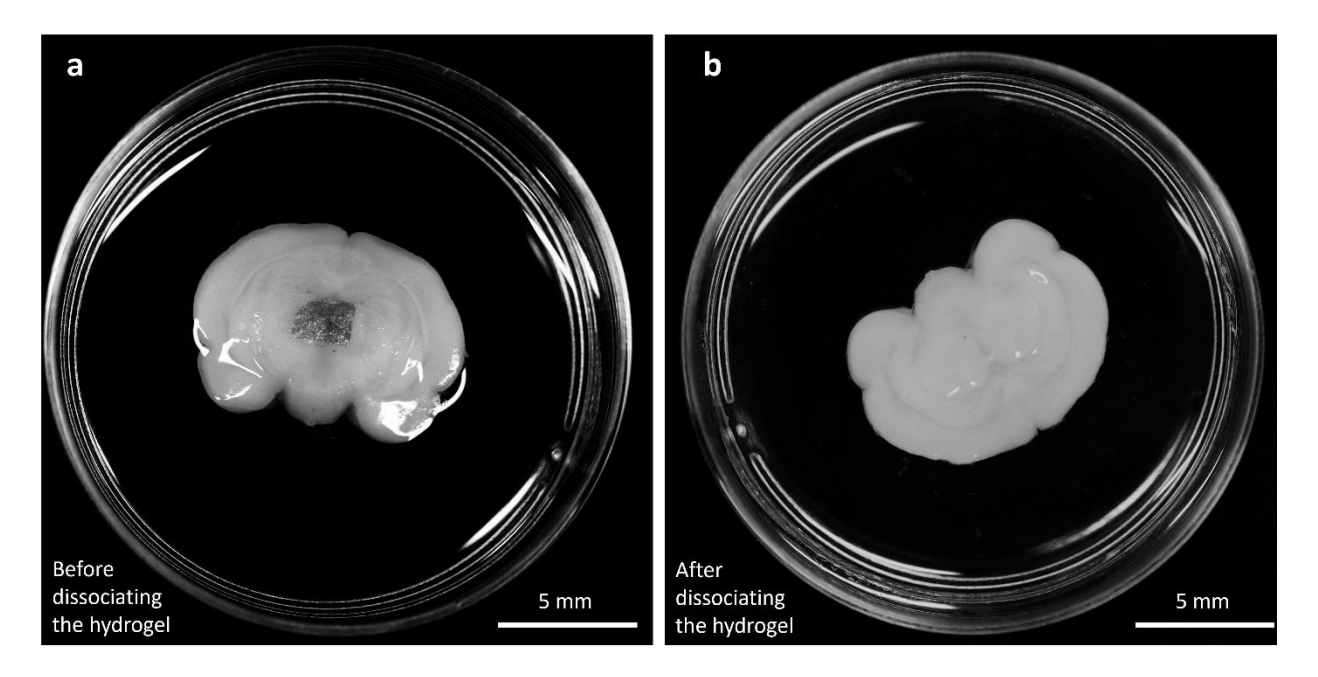


Figure S5. Characterization of the biotransfer printed Au NIL-wires on a rat brain slice. (a) Optical image of the Au NIL-wires on a rat brain slice before dissociating the alginate hydrogel. (b) Optical image of the Au NIL-wires on a rat brain slice after dissociating the alginate hydrogel with 20 mM EDTA.

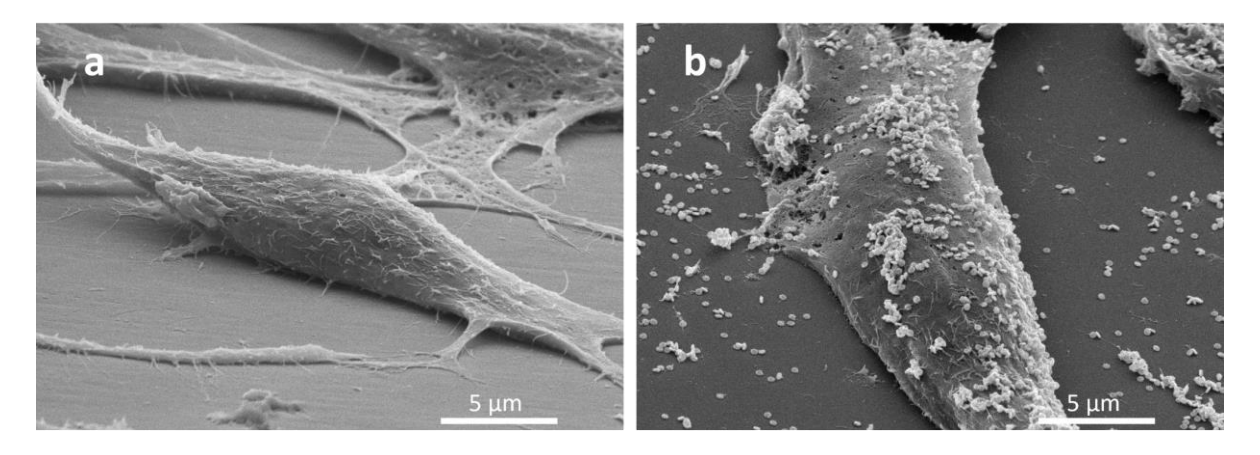


Figure S6. SEM images of NIH/3T3-GFP fibroblasts. a) SEM image of cells without Au NIL-arrays on a glass coverslip, b) SEM image of distorted Au NIL-dots on cells that were cultured for 4 hours.

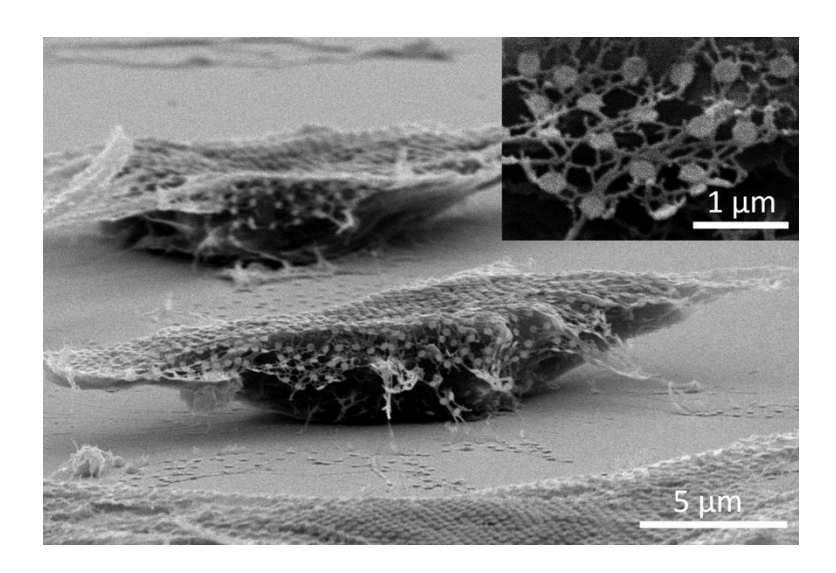


Figure S7. SEM image of NIH/3T3-GFP fibroblasts covered with a thin, porous film and Au NIL-dots.

Supplementary movie S1: Zoomed-in video clip of live cell imaging assembled from images captured over a period of 16.1 hours at 5-minute intervals with the Nikon TE2000 microscope. The clip shows an NIH/3T3-GFP cell with Au NIL-wires biotransfer printed on top. The cell appears healthy and able to migrate indicating biocompatibility of the transfer process, and the Au NIL-wires move with the cell during migration over this 16 hr period.

Supplementary movie S2: Zoomed-in video clip of live cell imaging assembled from images captured over a period of 16.1 hours at 5-minute intervals with the Nikon TE2000 microscope. The clip shows a different NIH/3T3-GFP cell with Au NIL-wires biotransfer printed on top. The cell appears healthy and able to migrate indicating biocompatibility of the transfer process, and the Au NIL-wires move with the cell during migration over this 16 hr period.

Supplementary movie S3: Large area video clip of live cell imaging assembled from images captured over a period of 16.1 hours at 5-minute intervals using the Nikon TE2000 microscope. The clip shows NIH/3T3-GFP cells with Au NIL-wires biotransfer printed on top. The cells with NIL-wires appear healthy and able to migrate indicating biocompatibility of the transfer process. Au NIL-wires adhere to some cells and move with them during migration over this 16 hr period. The images were taken with a 10X objective lens.

References

- (1) Chaudhuri, O.; Gu, L.; Klumpers, D.; Darnell, M.; Bencherif, S. A.; Weaver, J. C.; Huebsch, N.; Lee, H.-P.; Lippens, E.; Duda, G. N.; Mooney, D. J. Hydrogels with Tunable Stress Relaxation Regulate Stem Cell Fate and Activity. *Nat. Mater.* **2016**, *15* (3), 326–334.
- (2) Piccinini, F; Kiss, A.; Horvath, P. CellTracker (not only) for dummies. *Bioinformatics* **2015**, *32* (6), 955–957.